THE JOURNAL OF PHYSICAL CHEMISTRY LETTERS
A JOURNAL OF THE AMERICAN CHEMICAL SOCIETY

pubs.acs.org/JPCL

Letter

High-Throughput Screening of Element-Doped Carbon Nanotubes Toward an Optimal One-Dimensional Superconductor

Tao Bo, Yanan Wang, Yingzong Liang, Xinbao Liu, Jun Ren, Hongming Weng, Miao Liu,* and Sheng Meng*

Cite This: *J. Phys. Chem. Lett.* 2021, 12, 6667−6675

Read Online

ACCESS | Metrics & More | Article Recommendations | Supporting Information

ABSTRACT: In order to search for optimal one-dimensional (1D) superconductors with a high transition temperature (T_c), we performed high-throughput computation on the phonon dispersion, electron−phonon coupling (EPC), and superconducting properties of (5,0), (3,3), and element-doped (3,3) carbon nanotubes (CNTs) based on first-principles calculations. We find that the CNT (5,0) is superconductive with T_c of 7.9 K, while the (3,3) CNT has no superconductivity. However, by high-throughput screening of about 50 elements in the periodic table, we identified that 14 elemental dopants can make the (3,3) CNT dynamically stable and superconducting. The high $T_c \approx 28$ K suggests that the Si-doped (3,3) CNT is an excellent one-dimensional (1D) superconductor. In addition, the Al-, In-, and La-doped (3,3) CNTs are also great 1D superconductor candidates with a T_c of about 18, 17, and 29 K, respectively. These results may inspire the synthesis and discovery of optimal high-T_c 1D superconductors experimentally.

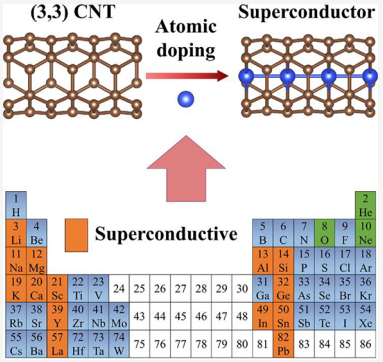

The discovery of copper oxides[1] and iron-based[2] unconventional superconductors has attracted tremendous attention in the past few decades, thanks to their high superconducting transition temperature T_c and great potential for quantum technological applications. Although considerable superconducting materials have been discovered, investigations focusing on one-dimensional (1D) superconductors are still rare. In recent years, a series of CrAs-based and Mo-based ternary superconductors with quasi-one-dimensional (Q1D) structures have been studied, including ACr_3As_3 and $A_2Cr_3As_3$ (A = Na, K, Rb, Cs),[3−8] $A_2Mo_6Se_6$ (A = Tl, In),[9] and $A_2Mo_3As_3$ (A = K, Cs, Rb).[10−12] Among these Q1D superconductors, $Cs_2Mo_3As_3$ possesses the highest T_c of 11.5 K.[11] Other Q1D nanowire superconductors such as Ta_2PdS_5 (T_c = 3.3 K),[13] Sn ($T_c \approx 4$ K),[14,15] and Al ($T_c < 1.6$ K)[16] have also been identified. However, these Q1D superconductors are actually bulk geometries with 1D atomic chains inside, not real 1D structures.

On the other hand, carbon nanotubes (CNTs) as ideal 1D materials have attracted tremendous attention since their discovery in 1991.[17] Researchers have paid attention to their potential superconductivity, with reports of experimental observations of superconductivity with a $T_c \approx 15$ K in 4 Å single-walled CNTs (SWCNTs),[18] $T_c \approx 0.55$ K in ropes of SWCNTs,[19] and $T_c \approx 12$ K in the multiwalled CNTs (MWCNTs).[20] While these studies are still under debate, there are an increasing number of studies focusing on superconductivity in CNTs.[21−25] The 4 Å SWCNTs were synthesized in the channels of porous zeolite crystals,[26,27] which include three types of tubes (e.g., (5,0), (3,3), and (4,2)).[28] In 2001, Tang et al.[18] reported that zeolite-inserted 4 Å SWCNTs possess superconductivity with $T_c \approx 15$ K. However, the type of tube plays a crucial role in the superconducting behavior, and the influence of the zeolite template remains unclear. Theoretical studies have also investigated the electronic structures and the associated EPC for various 4 Å SWCNTs.[22,25,29−31] The (4,2) CNT is semiconducting with a small indirect band gap of ∼0.2 eV.[28] The (3,3) CNT undergoes a Peierls transition with a high critical temperature (>240 K), thereby inhibiting its superconductivity.[30] The superconductivity of (5,0) CNT remains controversial, and different methods or models lead to distinct results. Connetable et al.[30] reported that (5,0) CNT undergoes a Peierls transition above room temperature indicating no superconductivity, while Barnett et al.[22] and Iyakutti et al.[25] reported that it is superconducting with T_c of around 1 and 22.7 K, respectively. With the continuous development of first-principles methods and computer technologies, some high-T_c superconductors, such as H_3S[32] and LaH_{10},[33] have been successfully predicted recently. Therefore, it is of great significance to use first-principles methods to investigate further the superconductivity of 4 Å SWCNTs.

Received: June 22, 2021
Accepted: July 11, 2021
Published: July 13, 2021

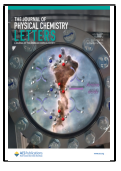

https://doi.org/10.1021/acs.jpclett.1c02000
J. Phys. Chem. Lett. 2021, 12, 6667−6675

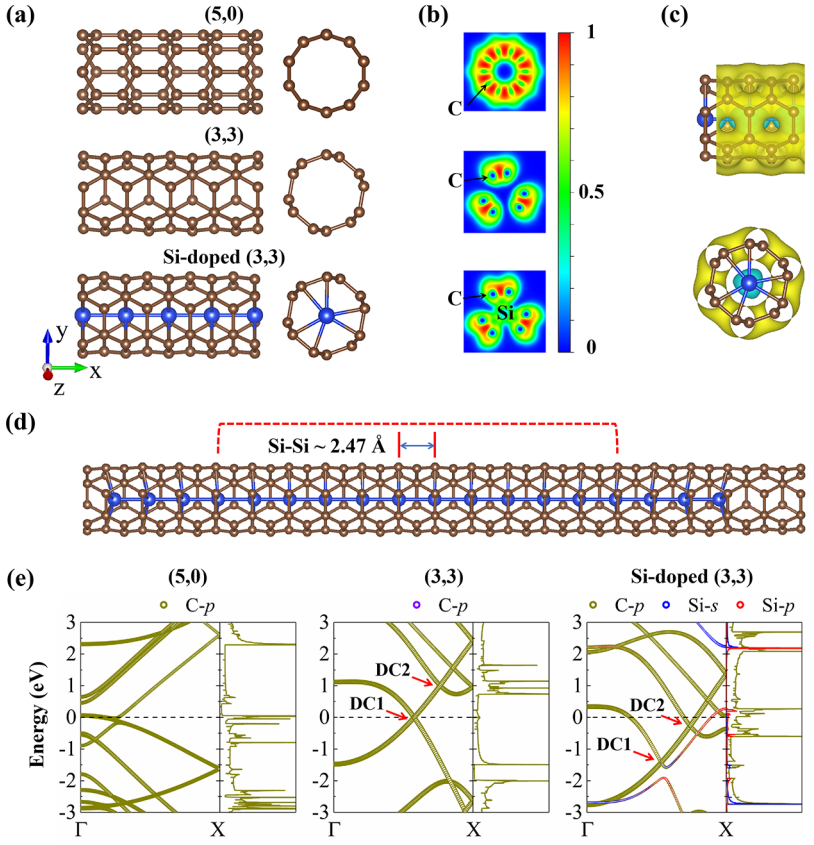

Figure 1. (a) Optimized structures and (b) ELF of (5,0), (3,3), and Si-doped (3,3) CNTs. The C and Si atoms are marked in brown and blue, respectively. (c) Differential charge density for the Si-doped (3,3) CNT. The yellow and cyan areas represent electron gains and losses. (d) Optimized supercell of Si-doped (3,3) CNT as well as the Si−Si bond length (Å). (e) Orbital-resolved band structures as well as the total and the partial EDOS of (5,0), (3,3), and Si-doped (3,3) CNTs.

In order to explore 1D superconductors with a high T_c, we consider whether element doping could tune the superconducting properties of CNTs. It is well-known that superconductivity is enhanced in graphite intercalated compounds (GICs)[34] and alkali-intercalated graphene.[35,36] Examples include C_6Yb and C_6Ca with T_c of 6.5 and 11.5 K, respectively,[34] and Ca-intercalated bilayer[35] and multilayer graphene[36] with T_c of 4 and 7 K, respectively. Besides, Haruyama et al.[37,38] fabricated thin films of boron-doped CNTs and found that they possess superconductivity with the T_c of 6 K, which can be increased up to 19 K by applying a small pressure. Lee et al.[39] reported a large enhancement in conductivity by doping K and Br in ropes of SWCNTs. Bohnen et al.[40] predicted that T_c can be enhanced for (3,3) CNTs by intercalating Li to the nanotube-zeolite complex.

In this letter, in order to search for excellent 1D superconductors with high T_c, we performed high-throughput computation on the superconductivity of element-doped (5,0) and (3,3) CNTs based on first-principles calculations. Our results show that many elements can be intercalated in (3,3) CNTs to form dynamically stable atomic wires. Elemental doping significantly suppresses the Peierls transition and leads to superconductivity in doped (3,3) CNT. In particular, upon the basis of the BCS theory,[41] we find that the Si-doped CNT possesses superconductivity with a high T_c of ∼28 K by analytically solving the McMillan−Allen−Dynes formula,[42−44] indicating that it is an excellent 1D superconductor.

We begin with a discussion of structural information on the pristine (5,0), the pristine (3,3), and the Si-doped (3,3) CNTs (see Figure 1a). The diameter and the length of the translational vector along the tube axis (LTA) are calculated to be 4.10 and 4.25 Å for the pristine (5,0) CNT and 4.21 and 2.46 Å for the pristine (3,3) CNT, respectively, which are very consistent with previous DFT results.[28] We have studied the dynamic stability of (5,0) CNT doped with a range of ∼50 elements in the periodic table and found that almost all of them are unstable. However, the (3,3) CNT maintains a good dynamic stability with various elements intercalated. Thus, we mainly focus on the element-doped (3,3) CNTs. When Si atoms are doped into the (3,3) CNT, the diameter and the LTA increase to 4.39 and 2.48 Å, respectively. The doped Si atoms form a 1D chain structure with the Si−Si bond length of 2.48 Å along the axis of the CNT. In order to obtain a more accurate Si−Si bond length, we have considered the 20 × 1 × 1 supercell of (3,3) CNT inserted with a free-ended chain of 18 Si atoms, as shown in the red bracket of Figure 1d. The average length of these Si−Si bonds is 2.47 Å, which is very close to the LTA (2.48 Å), indicating it is reasonable to use the unit cell structure to investigate the superconductivity of the Si-doped (3,3) CNT.

In order to study bonding properties of the Si-doped (3,3) CNT, we have performed analyses on the electron localization function (ELF)[45] (see Figure 1b), Bader charge,[46] and differential charge density (see Figure 1c). Results indicate that strong C−C and C−Si covalent bonds are formed in the Si-doped (3,3) CNT. Detailed discussions are in the Supporting Information (SI). Recently Liu et al.[47] investigated the energetics of intercalating Li atoms into the (5,0), (3,3),

https://doi.org/10.1021/acs.jpclett.1c02000
J. Phys. Chem. Lett. 2021, 12, 6667−6675

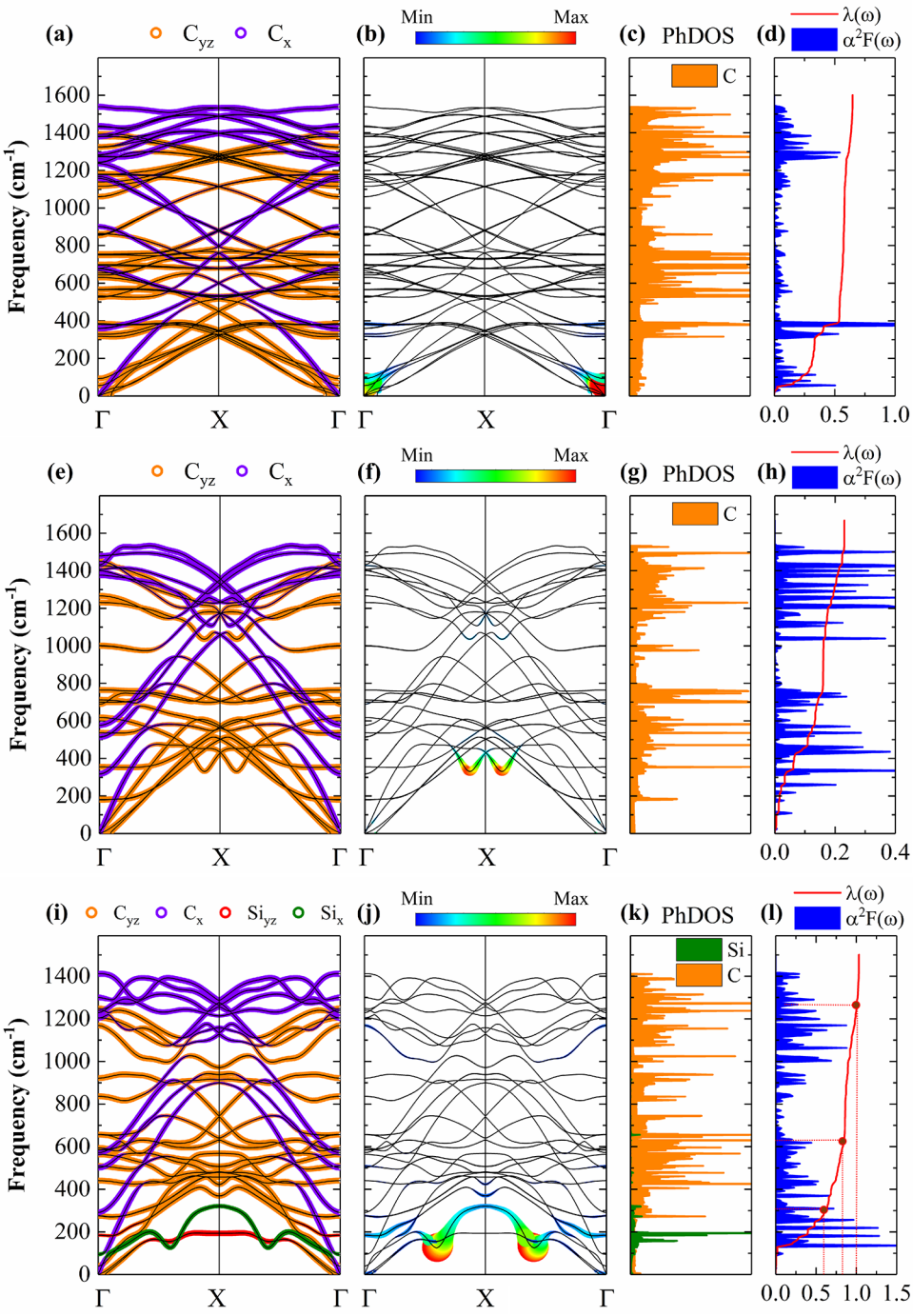

Figure 2. Phonon dispersions weighted by the motion modes of C and Si atoms of (a) the pristine (5,0), (e) the pristine (3,3), and (i) the Si-doped (3,3) CNTs. The purple, orange, green, and red colors represent C_x, C_{yz}, Si_x, and Si_{yz} modes, respectively. Phonon dispersions weighted by the magnitude of EPC λ_{qv} of (b) the pristine (5,0), (f) the pristine (3,3), and (j) the Si-doped (3,3) CNTs. PhDOS, Eliashberg spectral function $\alpha^2F(\omega)$, and cumulative frequency-dependent on EPC constant $\lambda(\omega)$ of (c–d) the pristine (5,0), (g–h) the pristine (3,3), and (k–l) the Si-doped (3,3) CNTs.

and (4,2) CNTs and found that it is possible for Li atoms doping into these 4 Å CNTs. In order to investigate the stability of the Si-doped (3,3) CNT, we have calculated the formation energy according to the following formula:

$$E_{form} = \frac{E_{Si@CNT} - E_{CNT} - E_{Si}}{N_{atom}} \quad (1)$$

where $E_{Si@CNT}$, E_{CNT}, and E_{Si} represent the total energies of the Si-doped (3,3) CNT, the pristine (3,3) CNT, and the isolated Si atom, respectively, and N_{atom} denotes the total number of atoms of the Si-doped (3,3) CNT. The formation energy of the Si-doped (3,3) CNT is 11.6 meV/atom, much smaller than the total energy difference between diamond and graphite (27 meV/atom).[48] It is known that the material synthesized experimentally is not limited to the one with the global minimum energy.[49] Once formed, the Si-doped (3,3) CNT is structurally stable since segregation of Si atoms is blocked by a high energy barrier >2.0 eV thanks to the strong covalent

https://doi.org/10.1021/acs.jpclett.1c02000
J. Phys. Chem. Lett. 2021, 12, 6667–6675

bonds between Si and C atoms. In addition, we have also investigated the dynamical stability of the Si-doped (3,3) CNT by calculating the phonon dispersion. No imaginary modes appearing in the Brillouin zone (BZ) confirms that the (3,3) CNT maintains good dynamical stability after Si doping. A detailed discussion on the phonon dispersion will be supplied later. The ab initio molecular dynamics (AIMD) simulations show that the Si-doped (3,3) CNT can maintain its original configuration with only slight deformations at temperatures up to 900 K, indicating excellent thermal stability (see Figures S1 and S2 of the Supporting Information). Detailed discussions are in the Supporting Information.

Figure 1e shows the orbital-resolved band structures as well as the electronic density of states (EDOS) of these three CNTs. Previous results show that both pristine (5,0) and (3,3) CNTs exhibit metallic characteristics.[28,47] For the pristine (5,0) CNT, there are two bands crossing the Fermi level. These two bands are almost flat near the Fermi level, resulting in a very large EDOS at the Fermi surface, which makes superconductivity possible. However, for the pristine (3,3) CNT, there are two bands forming a Dirac cone (labeled as DC1) at the Fermi level, similar to previous calculations.[29,40,47] The EDOS at the Fermi level is relatively small. In a previous study,[47] Liu et al. found that Li doping can increase the EDOS at the Fermi level of the (3,3) CNT. In this study, the bands move toward the lower energies in general after Si doping in the (3,3) CNT. The flat band around the Γ point moves from 1.1 to 0.3 eV, which is close to the Fermi level. The Dirac cone above the Fermi level (labeled as DC2) moved below the Fermi level, resulting in an extra band crossing the Fermi level. In addition, a new band crossing the Fermi level is formed near the X point, which is dominated by the Si-p orbitals. Because of the insertion of silicon atoms, the EDOS of the Fermi level is greatly increased, which will facilitate the superconductivity in the Si-doped (3,3) CNT.

To explore the possible superconductivity induced by EPC in the pristine (5,0), the pristine (3,3), and the Si-doped (3,3) CNTs, we have calculated the phonon dispersions, the phonon density of states (PhDOS), the Eliashberg electron−phonon spectral function $\alpha^2F(\omega)$, and the cumulative frequency-dependent on EPC constant $\lambda(\omega)$. As shown in Figure 2a,e, no imaginary phonon modes in the phonon dispersions indicates that both the pristine (5,0) and the pristine (3,3) CNTs are dynamically stable. For the tube (5,0), the low-frequency phonons (50−400 cm^{-1}) around the Γ point have a large contribution to the EPC λ_{qv} (see Figure 2b). In 1D systems, EPC often leads to the occurrence of Peierls transition, which can suppress superconductivity.[30] Barnett et al.[22] have investigated the Peierls transition of the (5,0) CNT with the Coulomb interaction and found that the Peierls transition is suppressed at a very low temperature, while the superconductivity becomes dominant at about 1 K. However, for the (3,3) CNT, several works reported that it undergoes a Peierls transition at a high temperature resulting from the phonon anomalies in certain phonon branches near $q = 2k_F$.[29,30] The Peierls transition might compete with the superconductivity. As shown in Figure 2e, we also find softened phonon modes in the range of 300−400 cm^{-1} around the X point, which is similar to previous results.[29,30] These softened phonon modes, mainly associated with the radial C_{yz} vibrations, contribute more to EPC λ_{qv} than other phonon modes (see Figure 2f).

Doping can not only change the electronic nature but also alter the phonon properties. Figure 2i shows that the phonon dispersion of the Si-doped (3,3) CNT has no imaginary phonon modes, indicating that the (3,3) CNT is dynamically stable after Si doping. Interestingly, several phonon branches of the Si-doped (3,3) CNT show the lower frequency in comparison with the pristine (3,3) CNT. The softened acoustic phonon branch with the second lowest frequency (~300 cm^{-1}) at the X point is mainly composed of axial Si_x vibrations. As shown in Figure 2j, this softened phonon branch has a large contribution to EPC λ_{qv}, indicating that Si doping can significantly enhance the EPC and improve the superconductivity of the (3,3) CNT.

The phonon density of states (PhDOS) are displayed in Figure 2c,g,k for the pristine (5,0), the pristine (3,3), and the Si-doped (3,3) CNTs, respectively. Figure 2k shows two regions of the PhDOS for the Si-doped (3,3) CNT: (I) 0−320 cm^{-1} and (II) above 320 cm^{-1}. In region I, both Si and C atoms play an important role since the acoustic phonon branches are composed of collective lattice modes of all atoms. In Region II, the spectral weight is primarily attributed as the vibrations of C atoms, due to the smaller atomic mass of C atoms than Si atoms. The calculated $\alpha^2F(\omega)$ and the EPC $\lambda(\omega)$ are displayed in Figure 2d,h,l for the pristine (5,0), the pristine (3,3), and the Si-doped (3,3) CNTs, respectively. Many peaks appear from the low-frequency to the high-frequency regions of the $\alpha^2F(\omega)$, for these pristine and Si-doped CNTs. Our calculated EPC constant λ for the pristine (5,0) CNT is 0.64, which is comparable with the previous value (0.57).[25] As shown in Figure 2d, there are two main frequency regions that have a great contribution to the EPC constant λ. The low-frequency phonon modes contribute 0.30 (47%) of the total EPC (λ = 0.64) below 150 cm^{-1}, and 0.25 (39%) between 300 and 400 cm^{-1}. For the pristine (3,3) CNT, the calculated EPC λ is very small (λ = 0.22). Because of Si doping, the EPC becomes stronger, and the total EPC λ increases to 1.01 from 0.22. As shown in Figure 2l, the low-frequency phonon modes below 300 cm^{-1}, mainly associated with Si_x and Si_{yz} vibrations, contribute 0.59 (58%) of the total EPC (λ = 1.01). The phonon modes above 300 cm^{-1}, primarily associated with C_x and C_{yz} vibrations, contribute 0.42 (42%) of the total EPC. Such behaviors have been found in many two-dimensional (2D) materials, such as 2D boron[50] and MB_6 monolayers,[51] where the most significant contribution to the EPC comes from the low-energy phonon modes.

The calculated T_c of about 0.05 K means that the pristine (3,3) CNT has almost no superconductivity, which is consistent with many previous theoretical results.[29,30] Our calculations show that the pristine (5,0) CNT is superconducting with T_c = 7.9 K. In the previous theoretical work, Iyakutti et al.[25] reported that the (5,0) CNT has superconductivity with T_c = 22.7 K. The higher T_c value is due to the use of the empirical value of the Debye temperature θ_D = 1400 K, which might be overestimated.[52] Interestingly, the T_c of the Si-doped (3,3) CNT reaches 28.0 K, much larger than that of the (5,0) tube (7.9 K), indicating that elemental doping can significantly improve the T_c. The influence of effective screened Coulomb repulsion μ^* on the T_c of these three CNTs are discussed in the Supporting Information (see Figure S3).

In order to evaluate the superconductivity of the Si-doped (3,3) CNT, we compare its EPC constant λ and T_c with those of other widely studied superconductors. The T_c of the Si-doped (3,3) CNT is not only higher than those of

https://doi.org/10.1021/acs.jpclett.1c02000
J. Phys. Chem. Lett. 2021, 12, 6667−6675

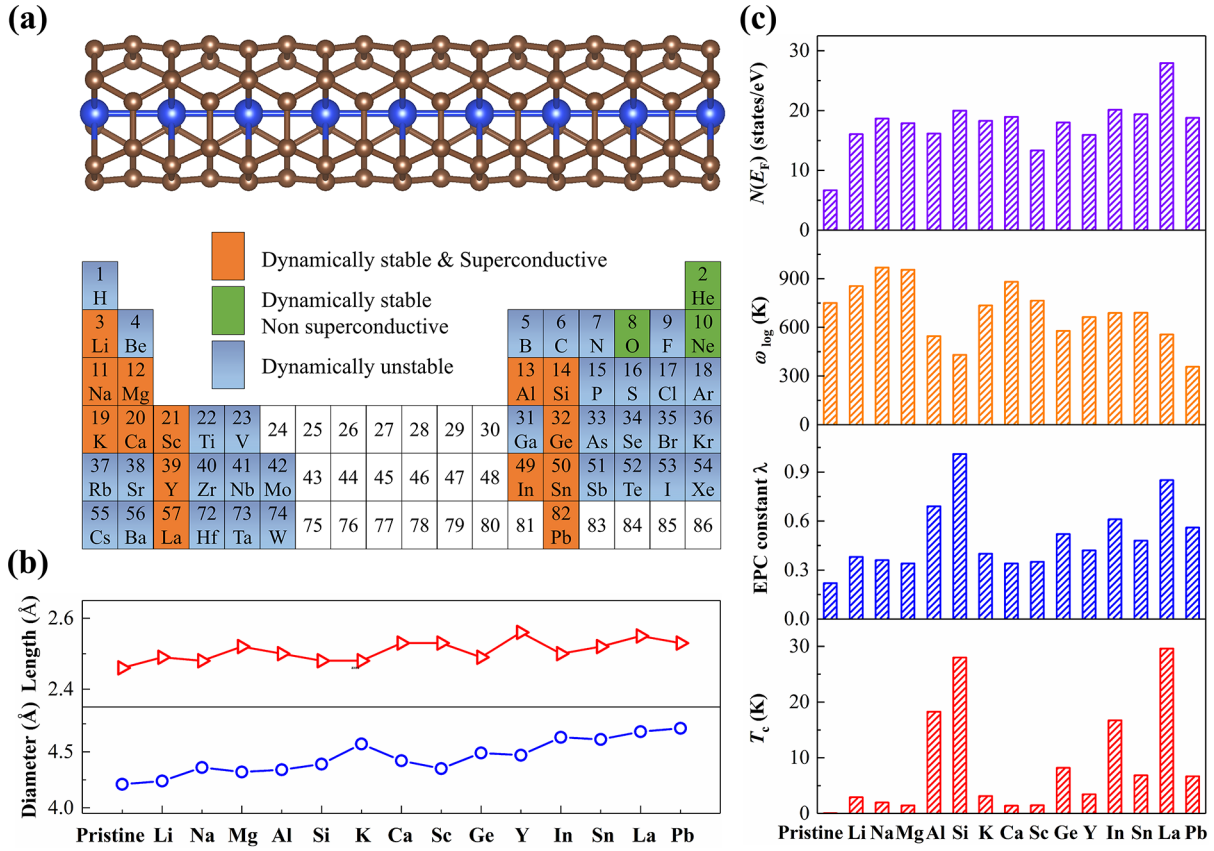

Figure 3. (a) All the dopants we have calculated in the periodic table of elements. The orange area indicates that the (3,3) CNT is dynamically stable and superconducting after doping. The green area denotes that the doped (3,3) CNT is dynamically stable but not superconducting, and the light blue area is dynamically unstable. (b) The axis length and the diameter of the (3,3) CNT after doping with various elements. (c) The $N(E_F)$, ω_{log}, lambda, and T_c for the (3,3) CNT after doping with various elements.

experimentally reported CNTs, including zeolite-inserted 4 Å SWCNTs (15 K),[18] ropes of SWCNTs (0.55 K),[19] and end-bonded MWCNTs (12 K),[20] but also higher than many Q1D superconductors, such as $Cs_2Mo_3As_3$ (T_c = 11.5 K),[11] Ta_2PdS_5 (T_c = 3.3 K),[13] Sn ($T_c \approx$ 4 K),[14,15] and Al (T_c < 1.6 K).[16] Besides, it is also higher than those of experimentally reported GICs[34,53,54] and alkali-intercalated graphene,[54−57] including GIC YbC_6 (6.5 K),[34] GIC CaC_6 (11.5 K),[34] Li-decorated graphene (5.9 K),[55] Ca-intercalated bilayer (4 K),[35] and multilayer (7 K)[36] graphene. The calculated EPC constant (λ = 1.01) of the Si-doped (3,3) CNT is larger than those of GICs[53,54] and alkali-intercalated graphene[54,56,57] ($0.33 \leq \lambda \leq 0.83$), which is responsible for its large T_c. On the basis of the above analysis, the Si-doped (3,3) CNT is an excellent 1D superconductor.

In order to study further the EPC and the superconductivity of doped (3,3) CNTs, we have tested about ∼50 elements from the periodic table of elements as the dopant, as shown in Figure 3a. High-throughput computation is performed for the structural properties, EPC, and superconducting properties of the (3,3) CNT doped with these elements. The colored areas represent the corresponding results with all the dopants we have calculated. The orange area indicates that the (3,3) CNT is dynamically stable and superconducting after doping. Therefore, we focus on the 14 elements, including Li, Na, Mg, Al, Si, K, Ca, Sc, Ge, Y, In, Sn, La, and Pb. The AIMD simulations show that these element-doped (3,3) CNTs possess excellent thermal stability except In-, Sn-, La-, and Pb-doped (3,3) CNTs. Detailed discussions are in the Supporting Information (see Figure S4). After the doping with these elements, the LTA and the diameter of the (3,3) CNT increase and have approximately a positive correlation with the radius of the doped atoms (see Figure 3b). The superconducting parameters of $N(E_F)$, ω_{log}, EPC constant λ, and T_c (K) for these element-doped (3,3) CNTs are presented in Figure 3c. The $N(E_F)$ increases significantly with dopants, indicating that doping increases the occupation of EDOS at the Fermi level. The large $N(E_F)$ value is helpful to the superconductivity of materials.[51] In addition, doping greatly improves the EPC constant λ of the (3,3) CNT. The calculated EPC constant λ is in the range of 0.34−1.01, which is much larger than that of the pristine (3,3) CNT (λ = 0.22). However, the calculated ω_{log} does not show an obvious increase after doping, and it even decreases for some elements. According to eq 7, T_c is related to both ω_{log} and EPC constant λ. We find that the (3,3) CNTs doped with Al, Si, In, and La, whose EPC constant λ are relatively large, possess a larger T_c (16.7−29.6 K) in comparison with other dopants. Figures S5−S7 show the phonon dispersion, the PhDOS, the $\alpha^2F(\omega)$, and the EPC constant $\lambda(\omega)$ of the Al-, In-, and La-doped (3,3) CNTs, respectively. Besides, the T_c of these 14 element-doped (3,3) CNTs using various effective screened Coulomb repulsion μ^* (0.05−0.15) is presented in Figure S8 of the Supporting Information. In general, doping suppresses the Peierls transition and leads to the superconductivity in the (3,3) CNT.

In summary, we have investigated the EPC and the superconducting properties of the pristine and the doped

https://doi.org/10.1021/acs.jpclett.1c02000
J. Phys. Chem. Lett. 2021, 12, 6667−6675

CNTs based on high-throughput first-principles calculations with the purpose of searching for optimal 1D superconductors with high T_c. Results show that the pristine (5,0) CNT is superconducting with T_c = 7.9 K, while the pristine (3,3) CNT has almost no superconductivity. However, the (3,3) CNTs doped with a set of 14 elements are dynamically stable and superconducting. In particular, the Si-doped (3,3) CNT does not show the imaginary phonon modes in the entire BZ. AIMD simulations show that the atomic geometry remains intact up to about 900 K, indicating the excellent thermal stability. Because of Si doping, the EDOS at the Fermi level is greatly increased, which is beneficial for the emergence of superconductivity. The corresponding T_c is determined to be ~28 K through the McMillan−Allen−Dynes formula, which is higher than those of other low-dimensional carbon-based superconductors, such as GICs, alkali-intercalated graphene, and $Cs_2Mo_3As_3$ Q1D superconductors, suggesting that the Si-doped (3,3) CNT is an excellent 1D superconductor. In addition, the Al-, In-, and La-doped (3,3) CNTs are also excellent 1D superconductor candidates with high T_c of about 18, 17, and 29 K, respectively. These results would inspire further explorations to discover and synthesize optimized 1D superconductors in the laboratory soon.

COMPUTATIONAL METHODS

The structural optimization, AIMD simulations, and charge density calculations are performed within the framework of density functional theory (DFT), based on Vienna Ab initio Simulation Package (VASP).[58] The supercell of CNTs with periodic boundary condition along the x-axis adopts a vacuum layer exceeding 15 Å along the y and z directions. The projector augmented wave (PAW) method[59] and Perdew−Burke−Ernzerhof (PBE) exchange-correlation functional[60] are employed, with a plane-wave cutoff of 600 eV and k-point mesh of (16 × 1 × 1) in the Monkhorst−Pack sampling scheme.[61] For geometric optimization, all atoms are allowed to fully relax until the forces on atoms are less than 0.005 eV/Å. AIMD simulations for the Si-doped (3,3) CNT are performed in (4 × 1 × 1) supercell models using DFT calculations. A time step of 1 fs is utilized. The structures are heated to targeted temperatures of 300, 900, and 1500 K at a constant rate by velocity scaling over a time period of 5 ps. The NVT ensemble using a Nosé−Hoover thermostat[62] is adopted.

The calculations of electronic structures, phonon dispersions, EPC, and superconducting properties are performed in the framework of DFT, employing norm-conserving pseudopotentials[63] as implemented in the QUANTUM-ESPRESSO (QE) package.[64] Before these calculations, the VASP-optimized structures are reoptimized within QE. The LTA and diameter calculated by QE and VASP are compared, and the results are almost the same (see Table S1). A plane-wave cutoff and the energy cutoff for charge density are set as 100 and 400 Ry, respectively. This set of parameters ensures a convergence less than 1 meV per formula unit in total energy. All structures are reoptimized until forces on each atom are less than 10^{-5} Ry/Bohr. The Brillouin zone (BZ) k-point mesh of 32 × 1 × 1 and a Methfessel-Paxton smearing width of 0.02 Ry are used to calculate the self-consistent electron density. The dynamic matrix and EPC matrix elements are computed within a 16 × 1 × 1 **q** mesh. The phonon properties and EPC are calculated based on the density functional perturbation theory[65] and Eliashberg theory.[66]

The EPC λ_{qv} is calculated according to the Migdal−Eliashberg theory[66] by

$$\lambda_{qv} = \frac{\gamma_{qv}}{\pi h N(E_F)\omega_{qv}^2} \tag{2}$$

where γ_{qv} is the phonon line width, $\omega_{qv}$is the phonon frequency, and $N(E_F)$ is the EDOS at the Fermi level. The γ_{qv} can be estimated by

$$\gamma_{qv} = \frac{2\pi\omega_{qv}}{\Omega_{BZ}} \sum_{k,n,m} \left| g^{v}_{kn,k+qm} \right|^2 \delta(\varepsilon_{kn} - E_F)\delta(\varepsilon_{k+qm} - E_F) \tag{3}$$

where Ω_{BZ} is the volume of BZ, ε_{kn} and ε_{k+qm} are the Kohn−Sham orbital energies, and $g^{v}_{kn,k+qm}$ represents the EPC matrix element. The Eliashberg spectral function $\alpha^2F(\omega)$ can be estimated by

$$\alpha^2F(\omega) = \frac{1}{2\pi N(E_F)} \sum_{qv} \frac{\gamma_{qv}}{h\omega_{qv}} \delta(\omega - \omega_{qv}) \tag{4}$$

Then, the EPC constant $\lambda(\omega)$ and the logarithmic average frequency $\omega_{log}(\omega)$ can be determined by

$$\lambda(\omega) = 2\int_0^{\omega} \frac{\alpha^2F(\omega)}{\omega}\, d\omega \tag{5}$$

and

$$\omega_{log}(\omega) = \exp\left[\frac{2}{\lambda}\int_0^{\infty} \frac{d\omega}{\omega}\alpha^2F(\omega)\log\omega\right] \tag{6}$$

After the total λ and ω_{log} are obtained, the T_c can be obtained by the McMillan equation,[42] which had been further modified by Allen and Dynes,[43,44]

$$T_c = \frac{\omega_{log}}{1.2} \exp\left[-\frac{1.04(1+\lambda)}{\lambda - \mu^*(1+0.62\lambda)}\right] \tag{7}$$

Here, μ^* is an empirical parameter that represents the effective screened Coulomb repulsion, which has a typical value between 0.1 and 0.15.[67] A detailed explanation of μ^* can be found in previous works.[51] The value of μ^* = 0.1 is widely used in theoretical calculations of the (5,0) CNT[25] and other superconducting materials, such as Al-deposited graphene AlC_8[68] and 2D boron-based materials.[50,69] Thus, we use the value of μ^* = 0.1 to discuss the superconducting properties.

ASSOCIATED CONTENT

Supporting Information

The Supporting Information is available free of charge at https://pubs.acs.org/doi/10.1021/acs.jpclett.1c02000.

Discussion of bonding properties of the Si-doped (3,3) CNT; snapshots, variation of the free energy, and RDF for the Si-doped (3,3) CNT in the AIMD simulations; the T_c of the pristine (5,0), the pristine (3,3), and the Si-doped (3,3) CNTs as a function of Coulomb pseudopotential μ^*; the AIMD simulations of the element-doped (3,3) CNTs; the phonon dispersions, PhDOS, $\alpha^2F(\omega)$, and EPC constant $\lambda(\omega)$ of the Al-, In-, and La-doped (3,3) CNTs; the T_c of the 14 element-doped (3,3) CNTs using various Coulomb pseudopotentials μ^*; the LTA and diameter of the pristine (5,0), the pristine (3,3), and the Si-doped (3,3) CNTs calculated by QE and VASP (PDF)

https://doi.org/10.1021/acs.jpclett.1c02000
J. Phys. Chem. Lett. 2021, 12, 6667−6675

AUTHOR INFORMATION

Corresponding Authors

Miao Liu − *Songshan Lake Materials Laboratory, Dongguan, Guangdong 523808, China; Beijing National Laboratory for Condensed Matter Physics and Institute of Physics, Chinese Academy of Sciences, Beijing 100190, China;* orcid.org/0000-0002-1843-9519; Email: mliu@iphy.ac.cn

Sheng Meng − *Songshan Lake Materials Laboratory, Dongguan, Guangdong 523808, China; Beijing National Laboratory for Condensed Matter Physics and Institute of Physics, Chinese Academy of Sciences, Beijing 100190, China;* orcid.org/0000-0002-1553-1432; Email: smeng@iphy.ac.cn

Authors

Tao Bo − *Songshan Lake Materials Laboratory, Dongguan, Guangdong 523808, China; Beijing National Laboratory for Condensed Matter Physics and Institute of Physics, Chinese Academy of Sciences, Beijing 100190, China;* orcid.org/0000-0002-0154-5454

Yanan Wang − *Songshan Lake Materials Laboratory, Dongguan, Guangdong 523808, China; Beijing National Laboratory for Condensed Matter Physics and Institute of Physics, Chinese Academy of Sciences, Beijing 100190, China*

Yingzong Liang − *Songshan Lake Materials Laboratory, Dongguan, Guangdong 523808, China; Beijing National Laboratory for Condensed Matter Physics and Institute of Physics, Chinese Academy of Sciences, Beijing 100190, China*

Xinbao Liu − *Beijing National Laboratory for Condensed Matter Physics and Institute of Physics, Chinese Academy of Sciences, Beijing 100190, China*

Jun Ren − *State Key Laboratory of Low-Dimensional Quantum Physics, Department of Physics, Tsinghua University, Beijing 100084, China*

Hongming Weng − *Songshan Lake Materials Laboratory, Dongguan, Guangdong 523808, China; Beijing National Laboratory for Condensed Matter Physics and Institute of Physics, Chinese Academy of Sciences, Beijing 100190, China;* orcid.org/0000-0001-8021-9413

Complete contact information is available at: https://pubs.acs.org/10.1021/acs.jpclett.1c02000

Notes

The authors declare no competing financial interest.

ACKNOWLEDGMENTS

We acknowledge financial support from Guangdong Basic and Applied Basic Research Foundation under Grant No. 2019A1515110920, National Natural Science Foundation of China (Nos. 12025407, 91850120, 11774396, 11934003), National Key Research and Development Program of China (No. 2016YFA0300902), and "Strategic Priority Research Program (B)" of Chinese Academy of Sciences (Grant No. XDB330301).

REFERENCES

(1) Dagotto, E. Correlated Electrons in High-Temperature Superconductors. *Rev. Mod. Phys.* **1994**, *66*, 763−840.

(2) Dai, P. Antiferromagnetic Order and Spin Dynamics in Iron-Based Superconductors. *Rev. Mod. Phys.* **2015**, *87*, 855−896.

(3) Bao, J.-K.; Liu, J.-Y.; Ma, C.-W.; Meng, Z.-H.; Tang, Z.-T.; Sun, Y.-L.; Zhai, H.-F.; Jiang, H.; Bai, H.; Feng, C.-M.; et al. Superconductivity in Quasi-One-Dimensional $K_2Cr_3As_3$ with Significant Electron Correlations. *Phys. Rev. X* **2015**, *5*, 011013.

(4) Tang, Z.-T.; Bao, J.-K.; Liu, Y.; Sun, Y.-L.; Ablimit, A.; Zhai, H.-F.; Jiang, H.; Feng, C.-M.; Xu, Z.-A.; Cao, G.-H. Unconventional Superconductivity in Quasi-One-Dimensional $Rb_2Cr_3As_3$. *Phys. Rev. B: Condens. Matter Mater. Phys.* **2015**, *91*, No. 020506(R).

(5) Tang, Z.-T.; Bao, J.-K.; Wang, Z.; Bai, H.; Jiang, H.; Liu, Y.; Zhai, H.-F.; Feng, C.-M.; Xu, Z.-A.; Cao, G.-H. Superconductivity in Quasi-One-Dimensional $Cs_2Cr_3As_3$ with Large Interchain Distance. *Sci. China Mater.* **2015**, *58*, 16−20.

(6) Mu, Q.-G.; Ruan, B.-B.; Pan, B.-J.; Liu, T.; Yu, J.; Zhao, K.; Chen, G.-F.; Ren, Z.-A. Superconductivity at 5 K in Quasi-One-Dimensional Cr-based KCr_3As_3 Single Crystals. *Phys. Rev. B: Condens. Matter Mater. Phys.* **2017**, *96*, 140504.

(7) Mu, Q.-G.; Ruan, B.-B.; Pan, B.-J.; Liu, T.; Yu, J.; Zhao, K.; Chen, G.-F.; Ren, Z.-A. Ion-Exchange Synthesis and Superconductivity at 8.6 K of $Na_2Cr_3As_3$ with Quasi-One-Dimensional Crystal Structure. *Phys. Rev. Mater.* **2018**, *2*, 034803.

(8) Liu, T.; Mu, Q.-G.; Pan, B.-J.; Yu, J.; Ruan, B.-B.; Zhao, K.; Chen, G.-F.; Ren, Z.-A. Superconductivity at 7.3 K in the 133-type Cr-based $RbCr_3As_3$ Single Crystals. *EPL* **2017**, *120*, 27006.

(9) Petrović, A. P.; Lortz, R.; Santi, G.; Decroux, M.; Monnard, H.; Fischer, Ø.; Boeri, L.; Andersen, O. K.; Kortus, J.; Salloum, D.; et al. Phonon Mode Spectroscopy, Electron-Phonon Coupling, and the Metal-Insulator Transition in Quasi-One-Dimensional $M_2Mo_6Se_6$. *Phys. Rev. B: Condens. Matter Mater. Phys.* **2010**, *82*, 235128.

(10) Mu, Q.-G.; Ruan, B.-B.; Zhao, K.; Pan, B.-J.; Liu, T.; Shan, L.; Chen, G.-F.; Ren, Z.-A. Superconductivity at 10.4 K in a Novel Quasi-One-Dimensional Ternary Molybdenum Pnictide $K_2Mo_3As_3$. *Sci. Bull.* **2018**, *63*, 952−956.

(11) Zhao, K.; Mu, Q.-G.; Ruan, B.-B.; Liu, T.; Pan, B.-J.; Zhou, M.-H.; Zhang, S.; Chen, G.-F.; Ren, Z.-A. Synthesis and Superconductivity of a Novel Quasi-One-Dimensional Ternary Molybdenum Pnictide $Cs_2Mo_3As_3$. *APL Mater.* **2020**, *8*, 031103.

(12) Zhao, K.; Mu, Q.-G.; Ruan, B.-B.; Zhou, M.-H.; Yang, Q.-S.; Liu, T.; Pan, B.-J.; Zhang, S.; Chen, G.-F.; Ren, Z.-A. A New Quasi-One-Dimensional Ternary Molybdenum Pnictide $Rb_2Mo_3As_3$ with Superconducting Transition at 10.5K. *Chin. Phys. Lett.* **2020**, *37*, 097401.

(13) Zhang, E.; Zhi, J.; Zou, Y. C.; Ye, Z.; Ai, L.; Shi, J.; Huang, C.; Liu, S.; Lin, Z.; Zheng, X.; et al. Signature of Quantum Griffiths Singularity State in a Layered Quasi-One-Dimensional Superconductor. *Nat. Commun.* **2018**, *9*, 4656.

(14) Tian, M.; Wang, J.; Kurtz, J. S.; Liu, Y.; Chan, M. H. W.; Mayer, T. S.; Mallouk, T. E. Dissipation in Quasi-One-Dimensional Superconducting Single-Crystal Sn Nanowires. *Phys. Rev. B: Condens. Matter Mater. Phys.* **2005**, *71*, 104521.

(15) Lozano, D. P.; Couet, S.; Petermann, C.; Hamoir, G.; Jochum, J. K.; Picot, T.; Menéndez, E.; Houben, K.; Joly, V.; Antohe, V. A.; et al. Experimental Observation of Electron-Phonon Coupling Enhancement in Sn Nanowires Caused by Phonon Confinement Effects. *Phys. Rev. B: Condens. Matter Mater. Phys.* **2019**, *99*, 064512.

(16) Altomare, F.; Chang, A. M.; Melloch, M. R.; Hong, Y.; Tu, C. W. Evidence for Macroscopic Quantum Tunneling of Phase Slips in Long One-Dimensional Superconducting Al Wires. *Phys. Rev. Lett.* **2006**, *97*, 017001.

(17) Lijima, S. Helical Microtubules of Graphitic Carbon. *Nature* **1991**, *354*, 56−58.

(18) Tang, Z. K.; Zhang, L.; Wang, N.; Zhang, X. X.; Wen, G. H.; Li, G. D.; Wang, J. N.; Chan, C. T.; Sheng, P. Superconductivity in 4 Angstrom Single-Walled Carbon Nanotubes. *Science* **2001**, *292*, 2462−2465.

(19) Kociak, M.; Kasumov, A. Y.; Gueron, S.; Reulet, B.; Khodos, II; Gorbatov, Y. B.; Volkov, V. T.; Vaccarini, L.; Bouchiat, H. Superconductivity in Ropes of Single-Walled Carbon Nanotubes. *Phys. Rev. Lett.* **2001**, *86*, 2416−2419.

(20) Takesue, I.; Haruyama, J.; Kobayashi, N.; Chiashi, S.; Maruyama, S.; Sugai, T.; Shinohara, H. Superconductivity in Entirely

End-Bonded Multiwalled Carbon Nanotubes. *Phys. Rev. Lett.* **2006**, *96*, 057001.
(21) Zhang, B.; Liu, Y.; Chen, Q.; Lai, Z.; Sheng, P. Observation of High T_c One Dimensional Superconductivity in 4Å Angstrom Carbon Nanotube Arrays. *AIP Adv.* **2017**, *7*, 025305.
(22) Barnett, R.; Demler, E.; Kaxiras, E. Electron-Phonon Interaction In Ultrasmall-Radius Carbon Nanotubes. *Phys. Rev. B: Condens. Matter Mater. Phys.* **2005**, *71*, 035429.
(23) Ferrier, M.; Kasumov, A.; Deblock, R.; Guéron, S.; Bouchiat, H. Induced and Intrinsic Superconductivity in Carbon Nanotubes. *J. Phys. D: Appl. Phys.* **2010**, *43*, 374003.
(24) Liang, S.-D. Bardeen−Cooper−Schrieffer Formalism of Superconductivity in Carbon Nanotubes. *Phys. B* **2008**, *403*, 2288−2292.
(25) Iyakutti, K.; Bodapati, A.; Peng, X.; Keblinski, P.; Nayak, S. K. Electronic Band Structure, Electron-Phonon Interaction, and Superconductivity of (5,5), (10,10), and (5,0) Carbon Nanotubes. *Phys. Rev. B: Condens. Matter Mater. Phys.* **2006**, *73*, 035413.
(26) Wang, N.; Tang, Z. K.; Li, G. D.; Chen, J. S. Single-Walled 4Å Carbon Nanotube Arrays. *Nature* **2000**, *408*, 50−51.
(27) Qin, L.-C.; Zhao, X.; Hirahara, K.; Miyamoto, Y.; Ando, Y.; Iijima, S. The Smallest Carbon Nanotube. *Nature* **2000**, *408*, 50.
(28) Liu, H. J.; Chan, C. T. Properties of 4Å Carbon Nanotubes from First-Principles Calculations. *Phys. Rev. B: Condens. Matter Mater. Phys.* **2002**, *66*, 115416.
(29) Bohnen, K. P.; Heid, R.; Liu, H. J.; Chan, C. T. Lattice Dynamics and Electron-Phonon Interaction in (3,3) Carbon Nanotubes. *Phys. Rev. Lett.* **2004**, *93*, 245501.
(30) Connetable, D.; Rignanese, G. M.; Charlier, J. C.; Blase, X. Room Temperature Peierls Distortion in Small Diameter Nanotubes. *Phys. Rev. Lett.* **2005**, *94*, 015503.
(31) Zhang, T.; Sun, M. Y.; Wang, Z.; Shi, W.; Sheng, P. Crossover from Peierls Distortion to One-Dimensional Superconductivity in Arrays of (5,0) Carbon Nanotubes. *Phys. Rev. B: Condens. Matter Mater. Phys.* **2011**, *84*, 245449.
(32) Li, Y.; Hao, J.; Liu, H.; Li, Y.; Ma, Y. The Metallization and Superconductivity of Dense Hydrogen Sulfide. *J. Chem. Phys.* **2014**, *140*, 174712.
(33) Liu, H.; Naumov, I. I.; Hoffmann, R.; Ashcroft, N. W.; Hemley, R. J. Potential High-T_c Superconducting Lanthanum and Yttrium Hydrides at High Pressure. *Proc. Natl. Acad. Sci. U. S. A.* **2017**, *114*, 6990.
(34) Weller, T. E.; Ellerby, M.; Saxena, S. S.; Smith, R. P.; Skipper, N. T. Superconductivity in the Intercalated Graphite Compounds C_6Yb and C_6Ca. *Nat. Phys.* **2005**, *1*, 39−41.
(35) Ichinokura, S.; Sugawara, K.; Takayama, A.; Takahashi, T.; Hasegawa, S. Superconducting Calcium-Intercalated Bilayer Graphene. *ACS Nano* **2016**, *10*, 2761−2765.
(36) Li, K.; Feng, X.; Zhang, W.; Ou, Y.; Chen, L.; He, K.; Wang, L.-L.; Guo, L.; Liu, G.; Xue, Q.-K.; et al. Superconductivity in Ca-Intercalated Epitaxial Graphene on Silicon Carbide. *Appl. Phys. Lett.* **2013**, *103*, 062601.
(37) Murata, N.; Haruyama, J.; Reppert, J.; Rao, A. M.; Koretsune, T.; Saito, S.; Matsudaira, M.; Yagi, Y. Superconductivity in Thin Films of Boron-Doped Carbon Nanotubes. *Phys. Rev. Lett.* **2008**, *101*, 027002.
(38) Haruyama, J.; Matsudaira, M.; Reppert, J.; Rao, A.; Koretsune, T.; Saito, S.; Sano, H.; Iye, Y. Superconductivity in Boron-Doped Carbon Nanotubes. *J. Supercond. Novel Magn.* **2011**, *24*, 111−120.
(39) Lee, R. S.; Kim, H. J.; Fischer, J. E.; Thess, A.; Smalley, R. E. Conductivity Enhancement in Single-Walled Carbon Nanotube Bundles Doped with K and Br. *Nature* **1997**, *388*, 255−257.
(40) Bohnen, K. P.; Heid, R.; Chan, C. T. Lattice Instability and Superconductivity in Electron Doped (3,3) Carbon Nanotubes. *J. Phys.: Condens. Matter* **2009**, *21*, 084206.
(41) Bardeen, J.; Cooper, L. N.; Schrieffer, J. R. Theory of Superconductivity. *Phys. Rev.* **1957**, *108*, 1175−1204.
(42) McMillan, W. L. Transition Temperature of Strong-Coupled Superconductors. *Phys. Rev.* **1968**, *167*, 331−344.
(43) Allen, P. B. Neutron Spectroscopy of Superconductors. *Phys. Rev. B* **1972**, *6*, 2577−2579.
(44) Allen, P. B.; Dynes, R. C. Transition Temperature of Strong-Coupled Superconductors Reanalyzed. *Phys. Rev. B* **1975**, *12*, 905−922.
(45) Savin, A.; Nesper, R.; Wengert, S.; Fässler, T. F. ELF: The Electron Localization Function. *Angew. Chem., Int. Ed. Engl.* **1997**, *36*, 1808−1832.
(46) Tang, W.; Sanville, E.; Henkelman, G. A Grid-Based Bader Analysis Algorithm without Lattice Bias. *J. Phys.: Condens. Matter* **2009**, *21*, 084204.
(47) Liu, H. J.; Chan, C. T. Chirality Dependence of the Energetics and Electronic Properties of Li-Intercalated 4Å Carbon Nanotubes. *Solid State Commun.* **2003**, *125*, 77−82.
(48) Wang, J.-T.; Chen, C.; Mizuseki, H. Body Centered Cubic Carbon BC_{14}: an All-sp^3 Bonded Full-Fledged Pentadiamond. *Phys. Rev. B: Condens. Matter Mater. Phys.* **2020**, *102*, 184106.
(49) Sun, Y.; Lv, J.; Xie, Y.; Liu, H.; Ma, Y. Route to a Superconducting Phase above Room Temperature in Electron-Doped Hydride Compounds under High Pressure. *Phys. Rev. Lett.* **2019**, *123*, 097001.
(50) Penev, E. S.; Kutana, A.; Yakobson, B. I. Can Two-dimensional Boron Superconduct? *Nano Lett.* **2016**, *16*, 2522−2526.
(51) Bo, T.; Liu, P.-F.; Yan, L.; Wang, B.-T. Electron-Phonon Coupling Superconductivity in Two-Dimensional Orthorhombic MB_6 (M = Mg, Ca, Ti, Y) and Hexagonal MB_6 (M = Mg, Ca, Sc, Ti). *Phys. Rev. Mater.* **2020**, *4*, 114802.
(52) Benedict, L. X.; Crespi, V. H.; Louie, S. G.; Cohen, M. L. Static Conductivity and Superconductivity of Carbon Nanotubes: Relations between Tubes and Sheets. *Phys. Rev. B: Condens. Matter Mater. Phys.* **1995**, *52*, 14935−14940.
(53) Calandra, M.; Mauri, F. Theoretical Explanation of Superconductivity in C_6Ca. *Phys. Rev. Lett.* **2005**, *95*, 237002.
(54) Profeta, G.; Calandra, M.; Mauri, F. Phonon-Mediated Superconductivity in Graphene by Lithium Deposition. *Nat. Phys.* **2012**, *8*, 131−134.
(55) Ludbrook, B. M.; Levy, G.; Nigge, P.; Zonno, M.; Schneider, M.; Dvorak, D. J.; Veenstra, C. N.; Zhdanovich, S.; Wong, D.; Dosanjh, P.; et al. Evidence for Superconductivity in Li-Decorated Monolayer Graphene. *Proc. Natl. Acad. Sci. U. S. A.* **2015**, *112*, 11795−11799.
(56) Zheng, J.-J.; Margine, E. R. First-Principles Calculations of the Superconducting Properties in Li-Decorated Monolayer Graphene within the Anisotropic Migdal-Eliashberg Formalism. *Phys. Rev. B: Condens. Matter Mater. Phys.* **2016**, *94*, 064509.
(57) Margine, E. R.; Lambert, H.; Giustino, F. Electron-Phonon Interaction and Pairing Mechanism in Superconducting Ca-Intercalated Bilayer Graphene. *Sci. Rep.* **2016**, *6*, 21414.
(58) Kresse, G.; Furthmüller, J. Efficient Iterative Schemes for Ab Initio Total-Energy Calculations Using a Plane-Wave Basis Set. *Phys. Rev. B: Condens. Matter Mater. Phys.* **1996**, *54*, 11169−11186.
(59) Blöchl, P. E. Projector Augmented-Wave Method. *Phys. Rev. B: Condens. Matter Mater. Phys.* **1994**, *50*, 17953−17979.
(60) Perdew, J. P.; Burke, K.; Ernzerhof, M. Generalized Gradient Approximation Made Simple. *Phys. Rev. Lett.* **1996**, *77*, 3865−3868.
(61) Monkhorst, H. J.; Pack, J. D. Special Points for Brillouin-Zone Integrations. *Phys. Rev. B* **1976**, *13*, 5188−5192.
(62) Nosé, S. A Unified Formulation of the Constant Temperature Molecular Dynamics Methods. *J. Chem. Phys.* **1984**, *81*, 511−519.
(63) Fuchs, M.; Scheffler, M. Ab Initio Pseudopotentials for Electronic Structure Calculations of Poly-Atomic Systems Using Density-Functional Theory. *Comput. Phys. Commun.* **1999**, *119*, 67−98.
(64) Giannozzi, P.; Baroni, S.; Bonini, N.; Calandra, M.; Car, R.; Cavazzoni, C.; Ceresoli, D.; Chiarotti, G. L.; Cococcioni, M.; Dabo, I.; et al. QUANTUM ESPRESSO: a Modular and Open-Source Software Project for Quantum Simulations of Materials. *J. Phys.: Condens. Matter* **2009**, *21*, 395502.

https://doi.org/10.1021/acs.jpclett.1c02000
J. Phys. Chem. Lett. 2021, 12, 6667−6675

(65) Baroni, S.; De Gironcoli, S.; Dal Corso, A.; Giannozzi, P. Phonons and Related Crystal Properties from Density-Functional Perturbation Theory. *Rev. Mod. Phys.* **2001**, *73*, 515−562.
(66) Luo, B.; Yao, Y.; Tian, E.; Song, H.; Wang, X.; Li, G.; Xi, K.; Li, B.; Song, H.; Li, L. Graphene-Like Monolayer Monoxides and Monochlorides. *Proc. Natl. Acad. Sci. U. S. A.* **2019**, *116*, 17213−17218.
(67) Gao, M.; Li, Q.-Z.; Yan, X.-W.; Wang, J. Prediction of Phonon-Mediated Superconductivity in Borophene. *Phys. Rev. B: Condens. Matter Mater. Phys.* **2017**, *95*, 024505.
(68) Lu, H.-Y.; Yang, Y.; Hao, L.; Wang, W.-S.; Geng, L.; Zheng, M.; Li, Y.; Jiao, N.; Zhang, P.; Ting, C. S. Phonon-Mediated Superconductivity in Aluminum-Deposited Graphene AlC_8. *Phys. Rev. B: Condens. Matter Mater. Phys.* **2020**, *101*, 214514.
(69) Cheng, C.; Sun, J.-T.; Liu, H.; Fu, H.-X.; Zhang, J.; Chen, X.-R.; Meng, S. Suppressed Superconductivity in Substrate-Supported B_{12} Borophene by Tensile Strain and Electron Doping. *2D Mater.* **2017**, *4*, 025032.

https://doi.org/10.1021/acs.jpclett.1c02000
J. Phys. Chem. Lett. 2021, 12, 6667−6675